Single-Cell RNA Sequencing of Peripheral Blood Reveals That Monocytes With High Cathepsin S Expression Aggravate Cerebral Ischemia-Reperfusion Injury

Lexing Xie
Xinqiao Hospital
Shuang Zhang
Xinqiao Hospital
Li Huang
Xinqiao Hospital
Zhouzhou Peng
Xinqiao Hospital
Hui Lu
Xinqiao Hospital
Qian He
Xinqiao Hospital
Linlin Hu
Xinqiao Hospital
Bingqiao Wang
Xinqiao Hospital
Baoliang Sun
The Second Affiliated Hospital; Key Laboratory of Cerebral Microcirculation in Universities of Shandong; Shandong First Medical University & Shandong Academy of Medical Sciences, Taian
Qingwu Yang (yangqwmlys@163.com)
Xinqiao Hospital
Qi Xie
Xinqiao Hospital

Research Article

Keywords: Cathepsin S1, Neuroinflammation2junctional adhesion molecule3, Blood-brain barrier4,stroke5

Posted Date: December 16th, 2021

DOI: https://doi.org/10.21203/rs.3.rs-1157587/v1

Abstract

Background: Stroke persists as a major cause of morbidity and mortality worldwide. After a stroke, peripheral immune cells are rapidly activated and then infiltrate the central nervous system to cause inflammation in the brain. However, it is not clear when and how these peripheral immune cells affect the central inflammatory response and whether there are intervention targets that can alleviate ischemia-reperfusion injury. In this study, we collected mouse peripheral blood samples at different time points after stroke for single-cell sequencing to reveal the dynamic changes in peripheral immune cells.

Methods: We performed single-cell sequencing on peripheral blood of mice at 1, 3, 7, and 14 days after ischemia-reperfusion to analyze the changes of subpopulations after cerebral ischemia-reperfusion; Real-time PCR, western blot and enzyme-linked immunoabsorbent assay were used to perform mRNA and protein levels verification; Immunoprecipitation verifies the interaction of proteins and between junctional adhesion molecule (JAM-A) and Cathepsin S (CTSS) protein, in vitro enzyme digestion and silver staining method to detect the protease digestion effect of CTSS.

Results: Peripheral monocyte subpopulations increased significantly after ischemia-reperfusion. Pseudo-time trajectory analysis and gene function analysis further suggested that CTSS may play an important role in regulating monocyte activation and leading to proteolysis. Next, we found that the expression of CTSS was significantly increased in monocytes after I/R in mice. Then, we used CTSS inhibitors and knockout mouse experiments to prove that inhibiting its expression can significantly reduce infarct volume and reduce blood–brain barrier (BBB) leakage. In addition, we found that CTSS destroys BBB by binding to JAM family proteins to cause them degradation.

Conclusion: Inhibition of Cathepsin S attenuated cerebral ischemia reperfusion injury and Cathepsin S can be used as a novel target for drug intervention after stroke.

Introduction

Stroke persists as a major cause of morbidity and mortality worldwide[1, 2]. After a stroke, innate immunity is rapidly activated to recognize a wide variety of molecular complexes that are perceived as foreign and potentially damaging (danger-associated molecular patterns (DAMPs)[3]. As resident cells in the brain, microglia are activated when receiving DAMP signals; then, these cells undergo morphological changes and secrete a variety of inflammatory factors[4, 5]. Moreover, peripheral immune cells can be detected in the brain within a few hours after the onset of stroke. Neutrophils are the first to infiltrate the central system and promote the development of inflammation in the lesion by releasing a variety of cytokines. Subsequently, lymphocytes are also mobilized to infiltrate into the brain, which together aggravate intracerebral inflammation in the acute phase after stroke[6]. In the subacute phase, brain injury can transform the immune system from an activated state to an inhibitory state. The main features are the decrease in lymphocyte and monocyte activity and the upregulation of the expression of anti-

inflammatory factors. However, there remain controversies and knowledge gaps as to when and how peripheral cells change function and about which functions will ultimately be beneficial[7].

In addition, immune therapy for stroke has focused primarily on reducing injury volume and improving functional outcomes. Several drugs targeting the immune system that were effective in preclinical studies have failed in clinical trials. Fingolimod, a sphingosine-1 phosphate receptor (S1PR) modulator that prevents lymphocyte egress from lymph nodes, was approved by the FDA for multiple sclerosis, and there is an ongoing study of fingolimod in stroke[8, 9]. Siponimod, another S1PR modulator, also blocks the egress of lymphocytes from lymphoid organs and has been demonstrated to reduce brain infiltration in an experimental stroke model[10]. However, some studies noticed that a large number of T cells infiltrated the brain 14 days after intraluminal middle cerebral artery occlusion (MCAO), and the number continued to increase thereafter[11]. When the egress of activated T cells from lymph nodes was inhibited by treating mice with fingolimod from days 6 to 13 after stroke onset, the number of CD4+ T cells and Treg cells markedly decreased without affecting other immune cell populations, and neurological recovery was delayed[12, 13].

Traditionally, peripheral immune cells are thought to play a deleterious role in acute ischemic stroke[14]. Depletion of these cells in the acute phase can alleviate brain injury induced by ischemia. However, recent studies have shown that these cells have anti-inflammatory functions, participate in angiogenesis, phagocytose necrotic neurons, and promote neurovascular repair[15, 16]. Therefore, peripheral immune cells play dual roles in ischemic stroke, depending mainly upon the microenvironment and the window of time after stroke.

In this study, we collected mouse peripheral blood samples at different time points after stroke for single-cell sequencing to reveal the dynamic changes in peripheral immune cells. The results showed that the proportion of monocyte subpopulations involved in the protease cleavage reaction significantly increased after stroke. In particular, cathepsin S (CTSS), a representative molecule of this cell subgroup, was highly expressed after stroke. We next used CTSS inhibitor and knockout (KO) mouse experiments to prove that inhibiting CTSS expression can significantly reduce infarct volume and blood–brain barrier (BBB) leakage, suggesting that CTSS can be used as a novel target for drug intervention after stroke.

Materials And Methods

Animals

Cathepsin S (CTSS) knockout (KO) mouse offspring of breeding pairs on a C57BL/6 background were previously generated by Cyagen Biosciences Inc. (Suzhou, China).C57BL/6 mice were provided by Army Medical University. All mice were raised in a clean environment with a light-controlled room (12 h light and 12 h dark cycle) at a temperature of 25 ± 2°C and free access to food and water. All experiments involving animals were performed in agreement with the guidelines of the National Institutes of Health on the care and use of animals and the Animal Management Committee of the Third Military Medical University.

Focal cerebral ischemia model and treatment with CTSS

Transient focal cerebral ischemia in mice was induced by intraluminal occlusion of the left middle cerebral artery (MCAO), as previously described[17]. Briefly, male mice (8–10 weeks, 20–25 g) were anesthetized with 1% pentobarbital sodium. A 2-cm length of rounded-tip nylon suture (Jialing, Shanghai, China) was inserted into the internal carotid artery, and then it was advanced to block the left middle cerebral artery. After 90 minutes of MCAO, the mice were allowed to recover for 1-7days. Except for artery occlusion, sham-operated mice underwent the same surgical procedure. The rectal temperature was generally controlled at 37.0±0.5°C during the operation. The CTSS inhibitor LY3000328 (HY-15533, MedChemExpress, NJ, USA)) was injected into young (8–12 weeks) C57 mice by intraperitoneal injection. All mice were randomly divided into two groups: the vehicle group (Veh), which received vehicle (corn oil, 10 mg/kg), and the CTSS-treated group (CTSS), which received CTSS (10 mg/kg)[18]; CTSS was diluted with corn oil.

Single-cell RNA-sequencing

Blood was taken from the eyeballs of mice after ischemia-reperfusion (I/R) for 1, 3, and 7 days for peripheral blood single-cell sequencing. Peripheral blood mononuclear cells (PBMCs) were isolated using Ficoll-Paque PLUS (GE healthcare) density gradient centrifugation. Cells were resuspended in RPMI media (Gibco, MA, United States) to obtain a single-cell suspension with high cell viability. Next, cells were stained with a live/death dye (DAPI) and dead cells were removed using fluorescence-activated cell sorting (FACS) [19]. Live cells were resuspended in PBS buffer and recounted using AO/PI double staining kit to ensure cell viability again. Finally, cell suspensions were processed for single-cell RNA-sequencing using the 10×-Genomics 3' v2 kit, as specified by the manufacturer's instructions [20]. About 1×10^4 cells from each condition were loaded in separate inlets of a 10× Genomics Chromium controller in order to create GEM emulsions. The targeted recovery was 6,000 cells per condition. Emulsions were used to perform reverse transcription, cDNA amplification and RNA-sequencing library preparation. Libraries were sequenced on the Illumina HiSeq 4000 platform, using 75 bp paired-end reads and loading one sample per sequencing lane.

Single-cell RNA-seq data analysis

Single-cell RNA-sequencing data were processed using the Cell Ranger Single-Cell Software Suite (version 3.0.2, 10×-Genomics) [20]. Each sample was aligned to the mouse reference genome (mm10) using the Cell ranger, and raw expression data were analysed by R (version 3.5.1). Then, Cells of all datasets were first analysed for their unique molecular identifier (UMI) and mitochondrial gene counts, and cells with low (<300) or high (>2500) UMI counts or high percentage of mitochondrial genes (>4%) were excluded from further analysis. Data were integrated in a standardized workflow as recommended by the developers of the "Seurat"-package [21], including data normalization, identification of variable genes, finding anchors for integration based on variable genes, integration of all datasets, scaling of data, principle component analysis (PCA), and unsupervised clustering with a resolution of 0.7 based on

Uniform Manifold Approximation and Projection (UMAP). Cell types were identified based on a marker gene panel and on differentially expressed genes (DEGs) in every cluster. DEGs were calculated by Wilcoxon rank sum test with Bonferroni correction for adjusted p-values. As recommended by the "Seurat" developers, data in feature plots, violin plots, heat maps and trajectories demonstrating features that vary across conditions were displayed based on the "RNA"-count slot, and data reflecting the entire dataset were displayed based on the "integrated" dataset. Gene ontology (GO) networks based on DEGs were created using the Functional Annotation Bioinformatics Microarray Analysis (DAVID) [22].

Pseudotime analysis

Cells were ordered into a branched pseudotime trajectory using Monocle 3 and restricting the analysis to the highly variable genes identified by Seurat. Monocle was used to test for a significant correlation between gene expression and pseudotime in each trajectory [23]. A gene was defined as significantly associated with pseudotime if its estimated *q* value was lower than 0.01.

Neurological deficit score

Neurological deficits after 3 days of reperfusion in each mouse were evaluated with a 5-point scoring system using the Longa score test as previously described[24]. The scoring standards were as follows: 0 = no neurologic deficit; 1 = failure to extend the contralateral forepaw fully; 2 = circling to the contralateral side; 3 = falling over to the contralateral side; and 4 = no spontaneous locomotor activity.

Infarct volume evaluation

After 3 days of reperfusion, eight mice from each group were decapitated, and then we removed their brains to measure infarct volume by TTC staining. The mouse brains were sliced into seven sections on average and exposed to a 2% 2,3,5-triphenyl-2H-tetrazolium chloride (TTC) solution (Sangong Biotech, Shanghai, China) for approximately 15 minutes in a 37°C incubator. The white areas were infarcted tissue, and normal brain tissue was stained red. We used Image-Pro Plus 6.0 to analyze infarct volume according to the following formula: Infarct volume (%) = (right hemisphere volume−uninfarcted volume of left side)/right hemisphere volume×100[25].

ELISA Analysis

The amount of CTSS in peripheral blood was measured using a Mouse CTSS Quantikine ELISA Kit (CUSABIO, Wuhan, China) according to the manufacturer's instruction.

Quantitative real-time PCR

Total RNA was extracted from mouse brain tissues with TRIzol reagent (Invitrogen, Carlsbad, CA), and RNA was reverse transcribed into DNA and quantified by SYBR RT-PCR according to the manufacturer's instructions (Takara, Japan). GAPDH was defined as control gene.The primer sequences were as follows: CTSS-forward: 5'-GAAGAAATCTTGTGTCGGATGG-3'; CTSS-reverse: 5'-CACAAGAACCCTGGTATTTCAC-

3';IL-1β-forward: 5'-GCAGCAGCACATCAACAAGAGC-3'; IL-1β reverse: 5'-AGGTCCACGGGAAAGACACAGG-3';IL-6 forward: 5'-CTCCCAACAGACCTGTCTATAC-3'; IL-6 reverse:5'-CCATTGCACAACTCTTTTCTCA-3; TNF forward: 5'-ATGTCTCAGCCTCTTCTCATTC-3; TNF reverse: 5'-GCTTGTCACTCGAATTTTGAGA-3.

Western blotting

The detailed protocol was as described in our previous article[26]. In brief, cerebral tissue on the infarct side was extracted, and protein was separated using protein lysate with EDTA-free protease inhibitor (Roche, Germany). Electrophoresis and membrane transfer were performed with 12% concentration SDS-PAGE and polyvinylidene fluoride membranes. We used 5% BSA-blocked membranes at room temperature for 2 h and then incubated the membranes with primary antibodies against the following targets overnight at 4°C: β-tubulin (1:1000, Abcam) and CTSS (1:500, Abcam). The membranes were incubated with HRP-conjugated goat anti-mouse secondary antibodies and goat anti-rabbit secondary antibodies for 1 h at room temperature. Finally, we used the enhanced chemiluminescence (ECL) substrate method to visualize the proteins at the membranes and ImageJ software to evaluate the grayscale values. Western blotting-related reagents were obtained from Beyotime.

Immunofluorescence staining

As described in detail in our previous article[27], mouse brain samples were fixed with PBS and 4% paraformaldehyde, and then brain tissue was cut into 30-μm slices after incubation in 4% paraformaldehyde and 30% sucrose, and were then fixed and dehydrated. The slices were blocked with 5% goat serum supplemented with 0.3% Triton-100 at room temperature for 1 h and placed in solutions of the following primary antibodies for incubation overnight at 4°C: CD31 (1/100, Abcam), Neu-N (1/100, abcam). Then, the slices were incubated with the corresponding fluorescent secondary antibodies: Alexa Fluor 488 (1:500, donkey anti-mouse), Alexa Fluor 647 (1:500, donkey anti-rabbit), and Alexa Fluor 555 (1:500, donkey anti-rat), Alexa Fluor 555 (1:500, donkey anti-goat), which were all purchased from Invitrogen (Carlsbad, CA, United States). The sections were then immersed in 6-diamidino-2-phenylindole (DAPI, 1:5000) for 15 minutes at room temperature. Finally, we used a confocal fluorescence microscope (Leica Sp5, Mannheim, Germany) to capture images, and the positive cells were quantified by ImageJ software in three different random fields.

RNA scope in situ hybridization

Brain tissue was fixed with PBS and 4% paraformaldehyde and then made into frozen sections. mRNA expression levels were detected using the mouse gene-specific probes CTSS and C1q according to the manufacturer's instructions for RNAscope® detection (Advanced Cell Diagnostics,CA, United States). Confocal microscopy and ImageJ software were used for image acquisition and analysis.

TUNEL staining

Apoptotic cells were demonstrated Using the In Situ Cell Death Detection Kit, Fluorescein (Roche,54421700),brain tissues were performed following the protocol specified by the manufacturer.

Immunoprecipitation

Combined JAM-A antibody with magnetic beads, then lysed the brain tissue of fresh wild-type mice and I/R3 days and incubated with JAM-A magnetic bead complex overnight at 4°C. Specific operation steps was following the protocol specified by the manufacturer (*Thermo Fisher* Scientific, 88288).

Vascular permeability quantitation

As described in detail in the study[28], in brief, after 3 days of reperfusion, Alexa 488-fluorescein thiocarbamoyl dextran (Sigma, Carlsbad, CA ,United States) was injected into wild-type (WT) or CTSS KO mice through the tail vein. After 10 minutes, brain tissues were removed, sliced into 10-μm sections and stained with fluorescent antibodies against CD31 (1:100, Santa Cruz Biotechnology) to visualize mouse vascular morphology. Slices were imaged with a Leica confocal fluorescence microscope as described above.

In vitro cleavage assays Cleavage of recombinant protein in vitro

We obtained recombinant inactive CTSS from (R&D Systems). Inactive CTSS was activated in (37°C)50mM sodium acetate,0.25M Nacl (PH 4.5, 7.2, 9.8), 5mM DTT for 1.5h. Then,activated CTSS was incubated with recombinant JAM-A(50463-M02H,R&D),JAM-B (50464-M02H, R&D), JAM-C (50465-M08H, R&D) in the presence or absence of the CTSS inhibitor (9uM) ,LY3000328 (HY-15533, MCE) for 20 min.The reaction was stopped by adding SDS and boiled at 95-100 °C for 7 min. Load each sub-sample in an equal amount for subsequent protein silver stain analysis.

Silver stain

These assays were described in detail previously [29]. We obtained Quick Silver Staining Kit from Beyitime(P0017S). After the electrophoresis is completed, take the gel and put it in about 100ml of fixing solution, and shake it on a shaker at room temperature for 20 minutes at a shaking speed of 60-70 rpm. Fixing for 2h to reduce the background. Discard the fixative, add 100ml of 30% ethanol, and shake on a shaker at room temperature for 10 minutes at a shaking speed of 60-70 rpm.Discard the original solution, add 200ml Milli-Q grade pure water or double distilled water, shake on a shaker at room temperature for 1 minute at a shaking speed of 60-70 rpm and reduplicate once. Discard water, add 100ml silver solution (1X), shake on a shaker at room temperature for 10 minutes at a shaking speed of 60-70 rpm. Discard the original solution, add 100ml Milli-Q grade pure water or double distilled water, and shake on a shaker at room temperature for 1-1.5 minutes at a shaking speed of 60-70 rpm.Discard the water, add 100ml of silver-stained color developing solution, shake for 3-10 minutes at room temperature on a shaker, until an ideal expected protein band appears, and the shaking speed is 60-70rpm. Discard the silver staining solution, add 100ml silver staining stop solution (1X), and shake on a shaker at room temperature for 10 minutes at a shaking speed of 60-70 rpm. It is normal for gas to be produced when it is terminated, and the gas produced is carbon dioxide. Discard the silver dye stop solution, add 100ml Milli-Q grade pure

water or double distilled water, shake on a shaker at room temperature for 2-5 minutes at a shaking speed of 60-70rpm.

Isolation of cells and flow cytometry analysis

The brain tissues of the control and ischemic reperfusion 3 days were broken up and incubated with papain and DNase for 30 minutes at 37°C. Horse serum was used to terminate the digestion, and the tissue was pipetted into a single-cell suspension. Then, the myelin sheath and tissue debris were removed with a solution (3 ml DMEM, 1 ml Percoll, 4 ml D-PBS), and the red blood cells were lysed; The single cells obtained were blocked with 10% FBS at room temperature, and then the corresponding primary antibodies (CD45) were added; finally, the samples were washed and analyzed by flow cytometry.

Statistical analysis

Data was shown as percentage or the mean ± SEM and using student's t-tests to assess the statistical differences between two groups. Comparisons among multiple samples were evaluated by one-way ANOVA. Statistical significance was set at $P<0.05$.

Results

Single-cell transcriptome profiling of peripheral blood immune cells in mice

To explore the dynamic changes in peripheral blood immune cells in mice after stroke and the relationship with ischemia, we collected fresh peripheral blood samples derived from mice with MCAO for 1, 7, 14 days and the control mice for single-cell sequencing **(Figure 1A)**.After filtering out cells with low quality, we obtained transcriptome datasets from 36,905 cells with an average of 9,000 cells for each sample at each time point. The cell clusters were annotated with expression of canonical marker genes. Major cell types comprising PBMCs could be well captured by scRNA-seq, including CD4+ T cells (CD4), CD8+ T cells (CD8), Treg (FOXP3), B cells (CD19), monocytes (CD68), natural killer (NK) cells (KLRB1), and proliferative cells (MKI67) **(Figure 1B)**. We found that compared with controls, MCAO-treatment mice showed an increased percentage of monocytes, while a decreased percentages of B cells. Other types of peripheral blood cells (proliferative cells, CD8+ T cells, Treg cells) account for less than 10% of the total cells, so their dynamic changes are not clear in this experiment **(Figure 1C)**.

In addition, we found 28 clusters representing different cell types using t-distributed stochastic neighbor embedding (t-SNE) analysis **(Figure 1D)**. The top 10 featured genes of each cluster were displayed in the heat map **(Figure S1 and Table S1)**. We further calculated the proportion of each cell subgroup at different ischemia-reperfusion time points **(Figure 1E)**. Then we divide it into four categories, which indicated that the proportion of cell subpopulations continues to rise (group 1) or continues to decline (group 2) with the prolonged perfusion time, etc **(Figure 1F)**, among them, the 2, 9, and 10 cell subgroups in group 1 showed an increasing trend **(Figure 1F)**. In particular, clusters 2 and 10 belong to monocyte

subgroups, which further confirms that monocytes and their subgroups continue to increase their expression after ischemia-reperfusion.

Pseudotime analysis reveals the dynamic changes of cell subpopulations

To understand the hypothetical developmental relationships that might exist within the monocyte and macrophage clusters, we performed trajectory analysis on clusters 2, 7, 10, and 18 using the Monocle algorithm. Two branch points were determined based on changes in monocytes gene expression and this was plotted in pseudotime. Clusters were superimposed on the monocle pseudotime plot and revealed that cluster 18 and 2 fell towards the beginning while cluster 7 on the tail of pseudotime **(Figure 2A-C).** Interestingly, the distribution of cluster 10 is located in the entire pseudo-time trajectory, suggesting that cluster 10 may play a key role in the differentiation process of monocytes **(Figure 2C)**.

Therefore, we checked the expression levels of the characteristic genes (including APOE, CSF1R and CTSS) in cluster 10 in the pseudo-time trajectory. We found that the expression levels of these genes were significantly increased **(Figure 2D)**, suggested that the them may be the key molecules in the activation process of monocytes after ischemia-reperfusion. On the contrary, the expression of characteristic genes in cluster 2 (including CCL6, CCR2, FN1 and CHIL3) gradually decreases with the pseudo-time trajectory **(Figure 2D)**, indicating that their effect in promoting monocyte activation was limited.

Gene functional analysis of each cell cluster

According to the previous data (Figure 2), we found that cluster 2 and 10 may play the key role in regulating the activation of monocytes. Thus, we further performed GO analysis on these subpopulations. Through biological process and molecular function analysis, we found that the biological functions of cluster 2 mainly focus on inflammation and toll-like receptor pathways (Figure 3A). In order to obtain the core genes that regulate the biological functions of the cluster 2, we merged the data and take the intersection. It was found that S100a8 and serum amyloid A-3 protein (Saa3) were the key regulatory genes in cluster 2 (Figure 3B). However, we excluded them in the follow-up study because the function of these two genes in stroke have been widely reported.

Then, we performed gene function analysis on the cluster 10. It was showed that the biological functions of this subgroup were mainly enriched for defense response, inflammatory response, proteoglycan binding and collagen binding (Figure 3C). We have also obtained the core gene that regulate cluster 10 by combining the results of biological process and molecular function analysis (Figure 3D). We found that Cathepsin S (CTSS) was the only molecule that can regulate inflammation and bind with collagen at the same time. Since the activation of inflammatory cells and the degradation of collagen in the blood-brain barrier after stroke are important pathological features, we speculated that CTSS may act on these two pathways to affect the outcome of stroke.

Besides, we also analyzed the molecular functions of other clusters and found that each group has its own different functions (Figure S2). In group 2, there are mainly T cell subgroups (including cluster 3,13

and 14) whose molecular functions were concentrated on ribosomal composition and RNA binding, suggesting that these molecules may be involved in transcriptional regulation of T cells,The main gene function enrichment in group 3 and 4 were related to the binding of antigen and MHC, and the activation of chemokines. The genes involved in these functions and their regulatory mechanisms remain to be resolved.

CTSS expression increases after stroke

To verify the results of single-cell sequencing, we detected the expression of CTSS in peripheral blood of mice by ELISA, and found that its expression increased after MCAO in C57BL/6N mice,which is consistent with our single-cell sequencing results. **(Figure 4A)**. Since the peripheral immune cells (monocytes, neutrophils, lymphocytes) would aggravate the neuroinflammation when they enter brain after the BBB is destroyed, the expression of CTSS could be evaluated in the central nervous system.Quantitative real-time PCR revealed highly increased CTSS mRNA in the ischemic brain 3 days to 7 days after stroke and gradually returned to baseline at 14 days,western blot analysis also indicated the protein expression increased after MCAO in mice **(Figure 4B and C)**.These results suggested that the expression of CTSS was significantly increased mainly in the acute and subacute phases.

Our single-cell sequencing results showed that CTSS was mainly derived from peripheral blood monocyte subpopulations, thus,we assessed the location of CTSS in the mouse brain and found that CTSS was colocalized with C1q (a marker of microglia/macrophages) via in situ hybridization analysis in mouse brains **(Figure 4D and E)**, which was consistent with a previous article reported that CTSS displayed tissue specific distribution,selectively expressed on Antigen Presenting Cells (APCs),including monocytes/macrophages, microglia and other cells. [30, 31]

In addition, we obtained from the Gene Expression Omnibus database (GSE16561) that the expression of CTSS in the peripheral blood of patients with stroke was obviously increased **(Figure 4F)**. These results confirmed that the expression of CTSS was significantly increased after stroke, which may be a potential target for intervention.

Ablation of CTSS ameliorates cerebral ischemic damage

We first verified the knockout efficiency of CTSS-KO mice by quantitative real-time PCR **(Figure 5A)**, and the results showed that the mRNA level of CTSS was significantly suppressed (close to 80%). Then, to determine the impact of CTSS on cerebral ischemic injury, male CTSS KO mice and their WT littermates were subjected to 90 minutes of ischemia followed by reperfusion for 3 days. TTC and Longa scores were respectively used to evaluate the area of cerebral infarction and neurological deficit in mice. The brain infarct areas of MCAO(TTC) CTSS KO mice were smaller than those of WT mice (relative to the contralateral hemisphere; $P < 0.05$) **(Figure 5B)**, and the neurological function score was also less than that of WT mice **(Figure 5C)**. Compared with WT mice, CTSS KO mice exhibited lower levels of neuronal apoptosis after MCAO. **(Figure 5D)**. Furthermore, BBB disruption is also an important feature for neurological disorders after stroke[32]. We found that ischemia-induced BBB leakage after stroke was

obviously decreased in CTSS KO mice via the reduced permeability of thiocarbamoyl dextrans compared with that in WT controls **(Figure 5E)**.

According to our data analysis in Figure 2, CTSS may be related to the activation and function of monocytes. Besides, some articles reported CTSS is involved in immune responses through major histocompatibility complex class II antigen presentation and inactivate key innate immunity proteins, such as β-defensins 2,3 and secretory leukocyte protease inhibitor[33].Thus, we speculated CTSS can reglute neuroinflammatory in mice after MCAO. We found that immune cell infiltration caused by ischemia was significantly reduced by the decrease in CD45 in the CTSS KO mice by flow cytometry **(Figure 5F)**. In addition, quantitative real-time PCR revealed the inflammatory factors IL-1β, IL-6, and TNF-α were significantly reduced after ischemia reperfusion **(Figure 5G-I)** which was consistent with the previous study reported that CTSS promotes the release of inflammatory factors IL-1[34] from macrophages and microglia [35]. These results showed that knockout of CTSS can relieve neuroinflammation after ischemia in mice.

Cathepsin S promotes BBB destruction through junctional protein cleavage

We found in previous experiments that inhibiting CTSS can alleviate stroke damage, but the specific molecular mechanism of CTSS is still unclear. So we predicted that there are multiple interacting proteins with CTSS through the interacting protein database, including HLAs, CD72, TLR9, etc **(Figure 6A)**. Among them, junctional adhesion molecules (JAMs) are one of the components of tight junction proteins and are critical for maintaining the integrity of the BBB. Then we confirmed the interaction between JAM-A and CTSS through CO-IP experiments of brain tissue, indicating that JAM is very likely to be one of the substrates of CTSS. Moreover, its interaction is enhanced after cerebral ischemia, which may be due to the increase of CTSS in the brain after stroke **(Figure 6B)**.In tumors, CTSS can increase tumor brain metastasis by degrading JAMs of the blood-brain barrier[29], thus we confirmed CTSS can increase the permeability of the blood-brain barrier after stroke by degrading JAMs in mice.

Cathepsin S is a lysosomal cysteine protease that exerts proteolysis activity across a wide range of pH in macrophages[33].Thus we verified that JAMs are substrates of CTSS and are active under conditions of acidic pH (4.5), neutral pH (6.0) and alkaline pH (9.8) via in vitro enzyme digestion experiments **(Figure 6C)**. JAM-A and JAM-B were cleaved into small fragments of approximately 25 kD by CTSS recombinant protein under neutral and acidic conditions and slightly cleaved under alkaline conditions JAM-C could not be cleaved under neutral and acidic conditions but was slightly cleaved under alkaline conditions. This is not consistent with the previous article JAM-A and JAM-B can be degraded under acidic conditions, but only JAM-B can be cut under neutral conditions. It may be due to the different conditions of tumor and stroke, and it was also discovered for the first time that the JAM family can be slightly cleaved by CTSS under alkaline conditions.[29] However, the cleavage of JAM was inhibited by a CTSS inhibitor, LY3000328,which was consistent with our expectations. These results indicated that CTSS inhibitors attenuate the destruction of the BBB by inhibiting the cleavage of JAM after stroke.

Pharmacological inhibition of CTSS alleviates cerebral ischemic damage in mice

All mice, including the inhibitor group (intraperitoneal injection of CTSS inhibitor, dissolved in corn oil) and control group (intraperitoneal injection of corn oil), were subjected to MCAO for 90 minutes and reperfusion for 3 days. The CTSS inhibitor significantly decreased infarct size and neurological deficits **(Figure 7A and B).** The permeability of the BBB in mice after MCAO was also reduced in the inhibitor group **(Figure 7C)**. These results suggest that pharmacological inhibition and deficiency of CTSS alleviates ischemic injury in mice.

Discussion

Single-cell RNA sequencing (scRNA-seq) has been widely used to characterize the dynamics of various cells to identify disease-related cell subgroups[36, 37]. Recent studies have revealed through peripheral blood single-cell sequencing technology that T cell subsets are involved in the regulation of AD and aging[38, 39], but there is still a lack of research on peripheral blood changes after stroke. According to the changes in the proportion of each cell subpopulation at different times of ischemia-reperfusion (I/R), we further divided the cells into four categories and first analyzed the continuously rising cell subpopulation in this study. The results showed that peripheral monocyte subpopulations increased significantly after I/R, which was consistent with previous reports. In particular, through pseudo-time trajectory analysis, we have obtained the key cell subpopulations that regulate monocyte activation, and this subpopulation was significantly enriched in the protease cleavage pathway through GO analysis. These results enhanced the understanding of the biological functions of monocytes after I/R.

Furthermore, we found that CTSS, a key molecule involved in the regulation of protease cleavage, was significantly highly expressed in monocytes after I/R. CTSS, as a lysosomal enzyme, is expressed in a wide variety of immune cells. CTSS plays a significant role in various intracellular and extracellular processes, including proteolysis and major histocompatibility complex (MHC) class II-mediated immune responses[40-42]. Dysregulated expression and activity of CTSS is linked to the pathogenesis of multiple diseases, including a number of conditions affecting the lungs, liver and heart[43-45]. Unlike other members of the lysosomal cathepsin family that require an acidic pH, CTSS has potent endoproteolytic activity in a broad range of pHs, [46] which indicates that CTSS is proteolytically active at the neutral pH found in the extracellular microenvironment. Previous research found that CTSS efficiently cleaved the junctional adhesion molecule (JAM) family members JAM-A, JAM-B and JAM-C at pH 4.5, the acidic pH of the lysosome, and maintained robust cleavage of JAM-B specifically at pH 6.0, the acidified pericellular pH measured in solid tumors. They also found that CTSS specifically mediates BBB transmigration through proteolytic processing of the JAM to accelerate breast-to-brain metastasis[29, 32].. This is similar to our results, confirming that CTSS destroys the BBB by degrading JAM family proteins over a broad pH range.

JAM family proteins are essential for maintaining the structural integrity of the BBB [47, 48]. A large number of previous studies have found that after stroke, metalloproteinase (MMP) family proteins (specifically MMP-2, MMP-7 and MMP-9), which are released from infiltrated immune cells, disrupt the BBB by degrading JAMs and other extracellular matrix proteins[32] [49]. Inhibition of peripheral immune

cell infiltration through blood replacement or fingolimod treatment can effectively reduce the expression of MMP proteins, thereby reducing I/R injury[10]. However, the protease cleavage activity of MMP proteins was sensitive to the pH value [50-53]. Whether the change in pH value during ischemia and reperfusion has an effect on MMP activity needs to be further evaluated. In this study, we found that CTSS degrades JAM family proteins over a broad pH range. Additionally, either the use of CTSS KO mouse models or the use of CTSS inhibitors can prevent the destruction of the BBB caused by JAM degradation, suggesting that CTSS is an important treatment target for I/R.

Although we found that CTSS may be an important molecule that aggravates the destruction of the BBB by peripheral immune cells, there is still a large amount of single-cell sequencing data that urgently needs to be deciphered. For example, the cluster 2 and 9 subgroups, which are highly expressed throughout the acute and chronic phases, have stroke-associated functions related to oxidative stress, Toll receptors and SH3/SH2 receptors. The cluster 1 and 4 subgroups increased in the acute phase but began to decrease after 7 days of ischemia, indicating that they are likely to participate in the recovery of stroke. Therefore, it is necessary to further verify that these groups of cells are involved in acute ischemia and chronic repair.

Conclusions

In summary, through single-cell sequencing at different time points in cerebral I/R mice, we found that cluster 10 was involved in the enzyme digestion process. In this group, CTSS was obviously highly expressed after stroke, and CTSS inhibitors or KO in mice alleviated the destruction of the BBB by inhibiting JAM cleavage and neuroinflammation. We conclude that CTSS inhibitors may serve as new targets for clinical brain ischemia protection therapy.

Abbreviations

CTSS: Cathepsin S; BBB: Blood-brain barrier; JAM: junctional adhesion molecule; JAM-A: junctional adhesion molecule-A; IL-1β: Interleukin-1β; IL-6: Interleukin-6; TNF-α: Tumor necrosis factor α; TLR4: Toll-like receptor 4;MCAO: Middle cerebral artery occlusion; WT: Wildtype; I/R: Ischemia reperfusion; KO: Knockout.

Declarations

Ethics approval and consent to participate

All experiments involving animals were performed in agreement with the guidelines of the National Institutes of Health on the care and use of animals and the Animal Management Committee of the Third Military Medical University.

Consent for publication

Not applicable.

Availability of data and materials

Not applicable.

Competing interests

The authors declare that they have no competing interests.

Funding

This work was supported by grant the Key Programs of National Natural Science Foundation of China (81830039), Science Fund for Creative Research Groups of the Natural Science Foundation of Chongqing (cstc2019jcyj-cxttX0005); Natural Science Foundation of Shandong Province (No. ZR2019ZD32).

Authors' contributions

QY and QX were responsible for experimental guidance and design,LX and SZ mainly completed the experiment and article writing.HL,ZP and LH analyzed the data.QH,BW and LH revised the manuscript.

Acknowledgments

Not applicable.

References

1. Wang W, Jiang B, Sun H, Ru X, Sun D, Wang L, et al. Prevalence, Incidence, and Mortality of Stroke in China: Results from a Nationwide Population-Based Survey of 480 687 Adults. Circulation. 2017;135(8):759-71.https://www.ncbi.nlm.nih.gov/pubmed/28052979

2. Macrez R, Ali C, Toutirais O, Le Mauff B, Defer G, Dirnagl U, et al. Stroke and the immune system: from pathophysiology to new therapeutic strategies. The Lancet Neurology. 2011;10(5):471-80

3. Matzinger P. Friendly and dangerous signals: is the tissue in control? Nat Immunol. 2007;8(1):11-3.https://www.ncbi.nlm.nih.gov/pubmed/17179963

4. Bune LT, Thaning P, Johansson PI, Bochsen L, Rosenmeier JB. Effects of nucleotides and nucleosides on coagulation. Blood Coagul Fibrinolysis. 2010;21(5):436-41.https://www.ncbi.nlm.nih.gov/pubmed/20389237

5. Burnstock G. Purinergic signalling and disorders of the central nervous system. Nat Rev Drug Discov. 2008;7(7):575-90.https://www.ncbi.nlm.nih.gov/pubmed/18591979

6. Petrovic-Djergovic D, Goonewardena SN, Pinsky DJ. Inflammatory Disequilibrium in Stroke. Circulation Research. 2016;119(1):142-58.<Go to ISI>://WOS:000378496500017

7. Liu Q, Jin WN, Liu Y, Shi K, Sun H, Zhang F, et al. Brain Ischemia Suppresses Immunity in the Periphery and Brain via Different Neurogenic Innervations. Immunity. 2017;46(3):474-87.https://www.ncbi.nlm.nih.gov/pubmed/28314594

8. Wei Y, Yemisci M, Kim HH, Yung LM, Shin HK, Hwang SK, et al. Fingolimod provides long-term protection in rodent models of cerebral ischemia. Ann Neurol. 2011;69(1):119-29.https://www.ncbi.nlm.nih.gov/pubmed/21280082

9. Tian DC, Shi K, Zhu Z, Yao J, Yang X, Su L, et al. Fingolimod enhances the efficacy of delayed alteplase administration in acute ischemic stroke by promoting anterograde reperfusion and retrograde collateral flow. Ann Neurol. 2018;84(5):717-28.https://www.ncbi.nlm.nih.gov/pubmed/30295338

10. Bobinger T, Manaenko A, Burkardt P, Beuscher V, Sprugel MI, Roeder SS, et al. Siponimod (BAF-312) Attenuates Perihemorrhagic Edema And Improves Survival in Experimental Intracerebral Hemorrhage. Stroke. 2019;50(11):3246-54.https://www.ncbi.nlm.nih.gov/pubmed/31558140

11. Schulze J, Gellrich J, Kirsch M, Dressel A, Vogelgesang A. Central Nervous System-Infiltrating T Lymphocytes in Stroke Are Activated via Their TCR (T-Cell Receptor) but Lack CD25 Expression. Stroke. 2021;52(9):2939-47.<Go to ISI>://WOS:000687824000040

12. Zera KA, Buckwalter MS. T cells direct microglial repair of white matter after stroke. Trends Neurosci. 2021.https://www.ncbi.nlm.nih.gov/pubmed/34332802

13. Dominguez-Villar M, Raddassi K, Danielsen AC, Guarnaccia J, Hafler DA. Fingolimod modulates T cell phenotype and regulatory T cell plasticity in vivo. J Autoimmun. 2019;96:40-9.https://www.ncbi.nlm.nih.gov/pubmed/30122421

14. Muhammad S, Barakat W, Stoyanov S, Murikinati S, Yang H, Tracey KJ, et al. The HMGB1 receptor RAGE mediates ischemic brain damage. J Neurosci. 2008;28(46):12023-31.https://www.ncbi.nlm.nih.gov/pubmed/19005067

15. Ye XH, Wu Y, Guo PP, Wang J, Yuan SY, Shang Y, et al. Lipoxin A4 analogue protects brain and reduces inflammation in a rat model of focal cerebral ischemia reperfusion. Brain Res. 2010;1323:174-83.https://www.ncbi.nlm.nih.gov/pubmed/20138164

16. Neumann J, Gunzer M, Gutzeit HO, Ullrich O, Reymann KG, Dinkel K. Microglia provide neuroprotection after ischemia. FASEB J. 2006;20(6):714-6.https://www.ncbi.nlm.nih.gov/pubmed/16473887

17. Deng Y, Chen D, Wang L, Gao F, Jin B, Lv H, et al. Silencing of Long Noncoding RNA Nespas Aggravates Microglial Cell Death and Neuroinflammation in Ischemic Stroke. Stroke. 2019;50(7):1850-8.https://www.ncbi.nlm.nih.gov/pubmed/31167620

18. Jadhav PK, Schiffler MA, Gavardinas K, Kim EJ, Matthews DP, Staszak MA, et al. Discovery of Cathepsin S Inhibitor LY3000328 for the Treatment of Abdominal Aortic Aneurysm. ACS Med Chem Lett.

2014;5(10):1138-42.https://www.ncbi.nlm.nih.gov/pubmed/25313327

19. Cano-Gamez E, Soskic B, Roumeliotis TI, So E, Smyth DJ, Baldrighi M, et al. Single-cell transcriptomics identifies an effectorness gradient shaping the response of CD4(+) T cells to cytokines. Nat Commun. 2020;11(1):1801.https://www.ncbi.nlm.nih.gov/pubmed/32286271

20. Zheng GX, Terry JM, Belgrader P, Ryvkin P, Bent ZW, Wilson R, et al. Massively parallel digital transcriptional profiling of single cells. Nat Commun. 2017;8:14049.https://www.ncbi.nlm.nih.gov/pubmed/28091601

21. Stuart T, Butler A, Hoffman P, Hafemeister C, Papalexi E, Mauck WM, 3rd, et al. Comprehensive Integration of Single-Cell Data. Cell. 2019;177(7):1888-902 e21.https://www.ncbi.nlm.nih.gov/pubmed/31178118

22. Huang da W, Sherman BT, Lempicki RA. Systematic and integrative analysis of large gene lists using DAVID bioinformatics resources. Nature protocols. 2009;4(1):44-57.https://www.ncbi.nlm.nih.gov/pubmed/19131956

23. Qiu X, Hill A, Packer J, Lin D, Ma YA, Trapnell C. Single-cell mRNA quantification and differential analysis with Census. Nature methods. 2017;14(3):309-15.https://www.ncbi.nlm.nih.gov/pubmed/28114287

24. Tao S, Jia M, Qiu T. Expression and role of CaMKII and Cx43 in a rat model of post-stroke depression. Exp Ther Med. 2019;18(3):2153-9.https://www.ncbi.nlm.nih.gov/pubmed/31410169

25. Zeng JX, Wang YM, Luo ZF, Chang LC, Yoo JS, Yang H, et al. TRIM9-Mediated Resolution of Neuroinflammation Confers Neuroprotection upon Ischemic Stroke in Mice. Cell Reports. 2019;27(2):549-+.<Go to ISI>://WOS:000463894100019

26. Meng Z, Zhao T, Zhou K, Zhong Q, Wang Y, Xiong X, et al. A20 Ameliorates Intracerebral Hemorrhage-Induced Inflammatory Injury by Regulating TRAF6 Polyubiquitination. J Immunol. 2017;198(2):820-31.https://www.ncbi.nlm.nih.gov/pubmed/27986908

27. Xiong XY, Liu L, Wang FX, Yang YR, Hao JW, Wang PF, et al. Toll-Like Receptor 4/MyD88-Mediated Signaling of Hepcidin Expression Causing Brain Iron Accumulation, Oxidative Injury, and Cognitive Impairment After Intracerebral Hemorrhage. Circulation. 2016;134(14):1025-38.https://www.ncbi.nlm.nih.gov/pubmed/27576776

28. Ozen I, Roth M, Barbariga M, Gaceb A, Deierborg T, Genove G, et al. Loss of Regulator of G-Protein Signaling 5 Leads to Neurovascular Protection in Stroke. Stroke. 2018;49(9):2182-90.https://www.ncbi.nlm.nih.gov/pubmed/30354999

29. Sevenich L, Bowman RL, Mason SD, Quail DF, Rapaport F, Elie BT, et al. Analysis of tumour- and stroma-supplied proteolytic networks reveals a brain-metastasis-promoting role for cathepsin S. Nat Cell

Biol. 2014;16(9):876-88.https://www.ncbi.nlm.nih.gov/pubmed/25086747

30. Chen SJ, Chen LH, Yeh YM, Lin CK, Lin PC, Huang HW, et al. Targeting lysosomal cysteine protease cathepsin S reveals immunomodulatory therapeutic strategy for oxaliplatin-induced peripheral neuropathy. Theranostics. 2021;11(10):4672-87.https://www.ncbi.nlm.nih.gov/pubmed/33754020

31. Clark AK, Malcangio M. Microglial signalling mechanisms: Cathepsin S and Fractalkine. Exp Neurol. 2012;234(2):283-92.https://www.ncbi.nlm.nih.gov/pubmed/21946268

32. Sandoval KE, Witt KA. Blood-brain barrier tight junction permeability and ischemic stroke. Neurobiol Dis. 2008;32(2):200-19.https://www.ncbi.nlm.nih.gov/pubmed/18790057

33. Doherty DF, Nath S, Poon J, Foronjy RF, Ohlmeyer M, Dabo AJ, et al. Protein Phosphatase 2A Reduces Cigarette Smoke-induced Cathepsin S and Loss of Lung Function. Am J Respir Crit Care Med. 2019;200(1):51-62.https://www.ncbi.nlm.nih.gov/pubmed/30641028

34. Hughes CS, Colhoun LM, Bains BK, Kilgour JD, Burden RE, Burrows JF, et al. Extracellular cathepsin S and intracellular caspase 1 activation are surrogate biomarkers of particulate-induced lysosomal disruption in macrophages. Part Fibre Toxicol. 2016;13:19.https://www.ncbi.nlm.nih.gov/pubmed/27108091

35. Seo Y, Kim HS, Kang I, Choi SW, Shin TH, Shin JH, et al. Cathepsin S Contributes to Microglia-Mediated Olfactory Dysfunction Through the Regulation of Cx3cl1-Cx3cr1 Axis in a Niemann-Pick Disease Type C1 Model. Glia. 2016;64(12):2291-305.<Go to ISI>://WOS:000386751100017

36. International Multiple Sclerosis Genetics C. Multiple sclerosis genomic map implicates peripheral immune cells and microglia in susceptibility. Science. 2019;365(6460).https://www.ncbi.nlm.nih.gov/pubmed/31604244

37. Gao Y, Li H, Li Z, Xie L, Liu X, Huang Z, et al. Single-Cell Analysis Reveals the Heterogeneity of Monocyte-Derived and Peripheral Type-2 Conventional Dendritic Cells. J Immunol. 2021;207(3):837-48.https://www.ncbi.nlm.nih.gov/pubmed/34282004

38. Xu H, Jia J. Single-Cell RNA Sequencing of Peripheral Blood Reveals Immune Cell Signatures in Alzheimer's Disease. Front Immunol. 2021;12:645666.https://www.ncbi.nlm.nih.gov/pubmed/34447367

39. Huang Z, Chen B, Liu X, Li H, Xie L, Gao Y, et al. Effects of sex and aging on the immune cell landscape as assessed by single-cell transcriptomic analysis. Proc Natl Acad Sci U S A. 2021;118(33).https://www.ncbi.nlm.nih.gov/pubmed/34385315

40. van Dalen FJ, Bakkum T, van Leeuwen T, Groenewold M, Deu E, Koster AJ, et al. Application of a Highly Selective Cathepsin S Two-step Activity-Based Probe in Multicolor Bio-Orthogonal Correlative Light-Electron Microscopy. Front Chem. 2020;8:628433.https://www.ncbi.nlm.nih.gov/pubmed/33644004

41. Shi GP, Villadangos JA, Dranoff G, Small C, Gu L, Haley KJ, et al. Cathepsin S required for normal MHC class II peptide loading and germinal center development. Immunity. 1999;10(2):197-206.https://www.ncbi.nlm.nih.gov/pubmed/10072072

42. Kim SJ, Schatzle S, Ahmed SS, Haap W, Jang SH, Gregersen PK, et al. Increased cathepsin S in Prdm1(-/-) dendritic cells alters the TFH cell repertoire and contributes to lupus. Nat Immunol. 2017;18(9):1016-24.https://www.ncbi.nlm.nih.gov/pubmed/28692065

43. Baugh M, Black D, Westwood P, Kinghorn E, McGregor K, Bruin J, et al. Therapeutic dosing of an orally active, selective cathepsin S inhibitor suppresses disease in models of autoimmunity. J Autoimmun. 2011;36(3-4):201-9.https://www.ncbi.nlm.nih.gov/pubmed/21439785

44. Sena BF, Figueiredo JL, Aikawa E. Cathepsin S As an inhibitor of Cardiovascular inflammation and Calcification in Chronic Kidney Disease. Front Cardiovasc Med. 2018;4.<Go to ISI>://WOS:000426132700001

45. Wilkinson RD, Young A, Burden RE, Williams R, Scott CJ. A bioavailable cathepsin S nitrile inhibitor abrogates tumor development. Mol Cancer. 2016;15:29.https://www.ncbi.nlm.nih.gov/pubmed/27097645

46. Vasiljeva O, Dolinar M, Pungercar JR, Turk V, Turk B. Recombinant human procathepsin S is capable of autocatalytic processing at neutral pH in the presence of glycosaminoglycans. Febs Lett. 2005;579(5):1285-90.<Go to ISI>://WOS:000227210600052

47. Jia W, Martin TA, Zhang G, Jiang WG. Junctional adhesion molecules in cerebral endothelial tight junction and brain metastasis. Anticancer Res. 2013;33(6):2353-9.https://www.ncbi.nlm.nih.gov/pubmed/23749882

48. Liu WY, Wang ZB, Zhang LC, Wei X, Li L. Tight junction in blood-brain barrier: an overview of structure, regulation, and regulator substances. CNS Neurosci Ther. 2012;18(8):609-15.https://www.ncbi.nlm.nih.gov/pubmed/22686334

49. Ludewig P, Sedlacik J, Gelderblom M, Bernreuther C, Korkusuz Y, Wagener C, et al. Carcinoembryonic antigen-related cell adhesion molecule 1 inhibits MMP-9-mediated blood-brain-barrier breakdown in a mouse model for ischemic stroke. Circ Res. 2013;113(8):1013-22.https://www.ncbi.nlm.nih.gov/pubmed/23780386

50. Abdul-Muneer PM, Schuetz H, Wang F, Skotak M, Jones J, Gorantla S, et al. Induction of oxidative and nitrosative damage leads to cerebrovascular inflammation in an animal model of mild traumatic brain injury induced by primary blast. Free Radic Biol Med. 2013;60:282-91.https://www.ncbi.nlm.nih.gov/pubmed/23466554

51. Chen F, Ohashi N, Li W, Eckman C, Nguyen JH. Disruptions of occludin and claudin-5 in brain endothelial cells in vitro and in brains of mice with acute liver failure. Hepatology. 2009;50(6):1914-

23.https://www.ncbi.nlm.nih.gov/pubmed/19821483

52. Yang Y, Estrada EY, Thompson JF, Liu WL, Rosenberg GA. Matrix metalloproteinase-mediated disruption of tight junction proteins in cerebral vessels is reversed by synthetic matrix metalloproteinase inhibitor in focal ischemia in rat. J Cerebr Blood F Met. 2007;27(4):697-709.<Go to ISI>://WOS:000245358800005

53. Hua D, Tang L, Wang W, Tang S, Yu L, Zhou X, et al. Improved Antiglioblastoma Activity and BBB Permeability by Conjugation of Paclitaxel to a Cell-Penetrative MMP-2-Cleavable Peptide. Adv Sci (Weinh). 2021;8(3):2001960.https://www.ncbi.nlm.nih.gov/pubmed/33552853

Figures

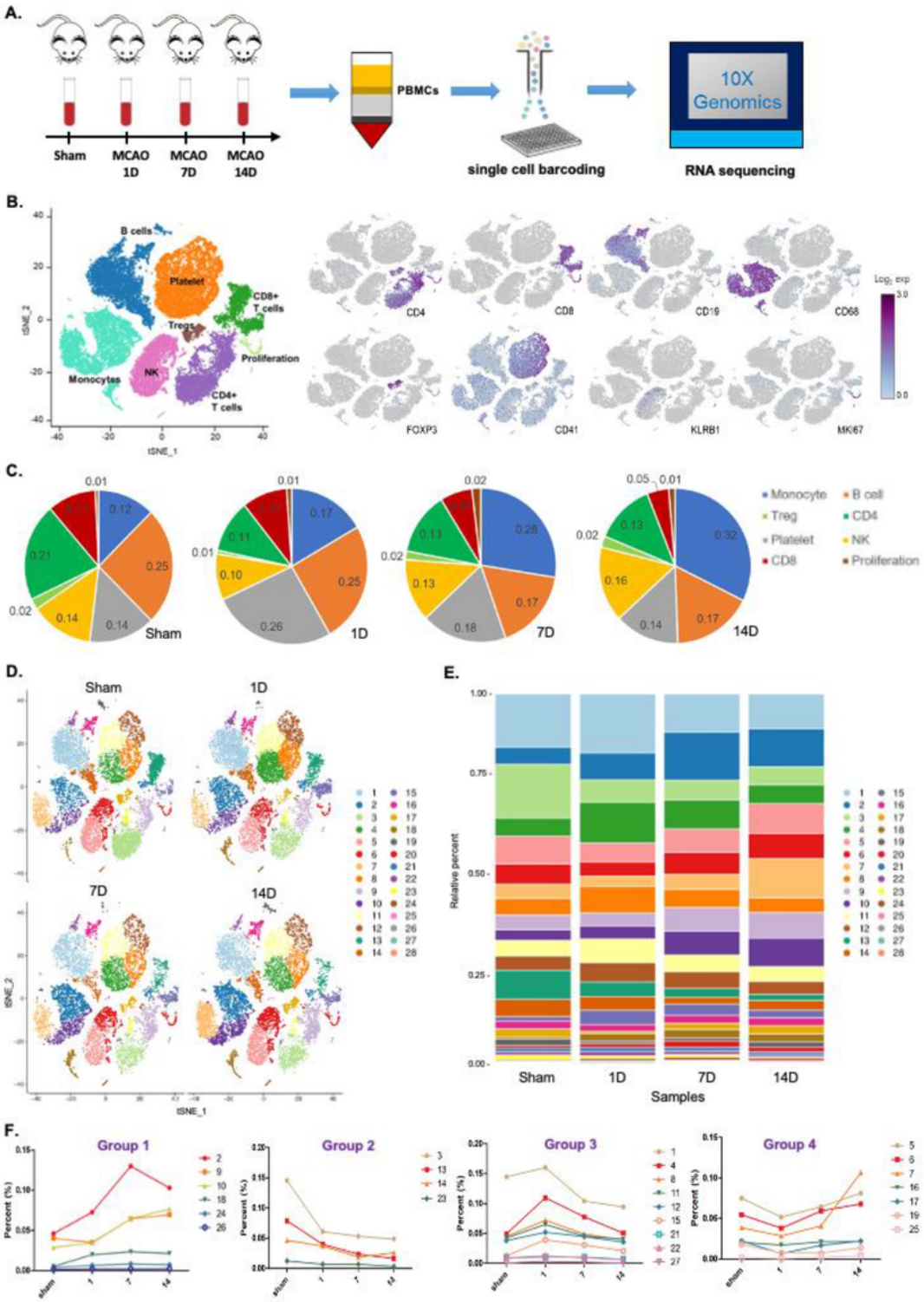

Figure 1

Single-cell gene expression analysis of peripheral blood immune cells in mice. (A) Experimental workflow for single-cell RNA analysis in the present study. (B) A total of eight cell types were shown in (B), including CD4+ T cells, CD8+ T cells, Tregs, Proliferation cells, B cells, Natural killer (NK) cells, platelet cells and monocyte cells. The canonical cell surface markers of the above cell population were shown on the right. (C) Proportion of the eight types of immune cells in the different samples. (D) tSNE analysis divides the

above cells into 28 cell subgroups. (E) Proportion of the 28 clusters of cells in the different samples. (F) Dynamic changes in a total of 28 clusters of cells.Dynamic changes in a total of 28 clusters of cells.

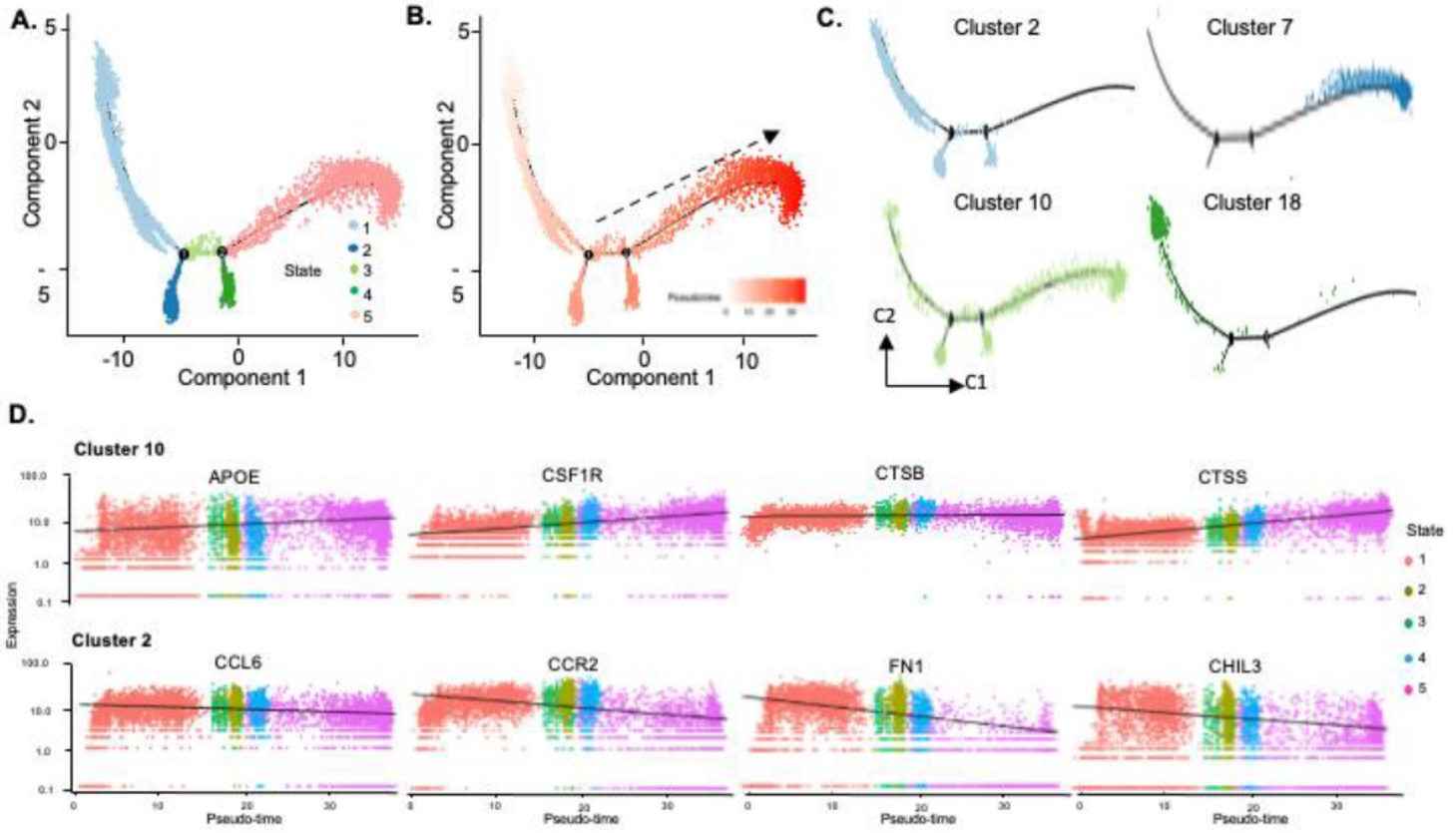

Figure 2

Pseudotime analysis reveals the dynamic changes of cell subpopulations from monocytes. (A) The monocyte cell subgroups were selected for trajectory reconstruction. Pseudotime reconstruction revealed a bifurcating trajectory of monocytes development. The coloring of individual cell along the optimized embedding path represents the different states of monocyte differentiation. (B) The direction indicated by the arrow represents the trajectory of monocyte differentiation. (C) Distribution of different clusters of monocytes on the differentiation trajectory. (D) Dynamic changes in the expression of core genes involved in regulating the differentiation of different clusters.

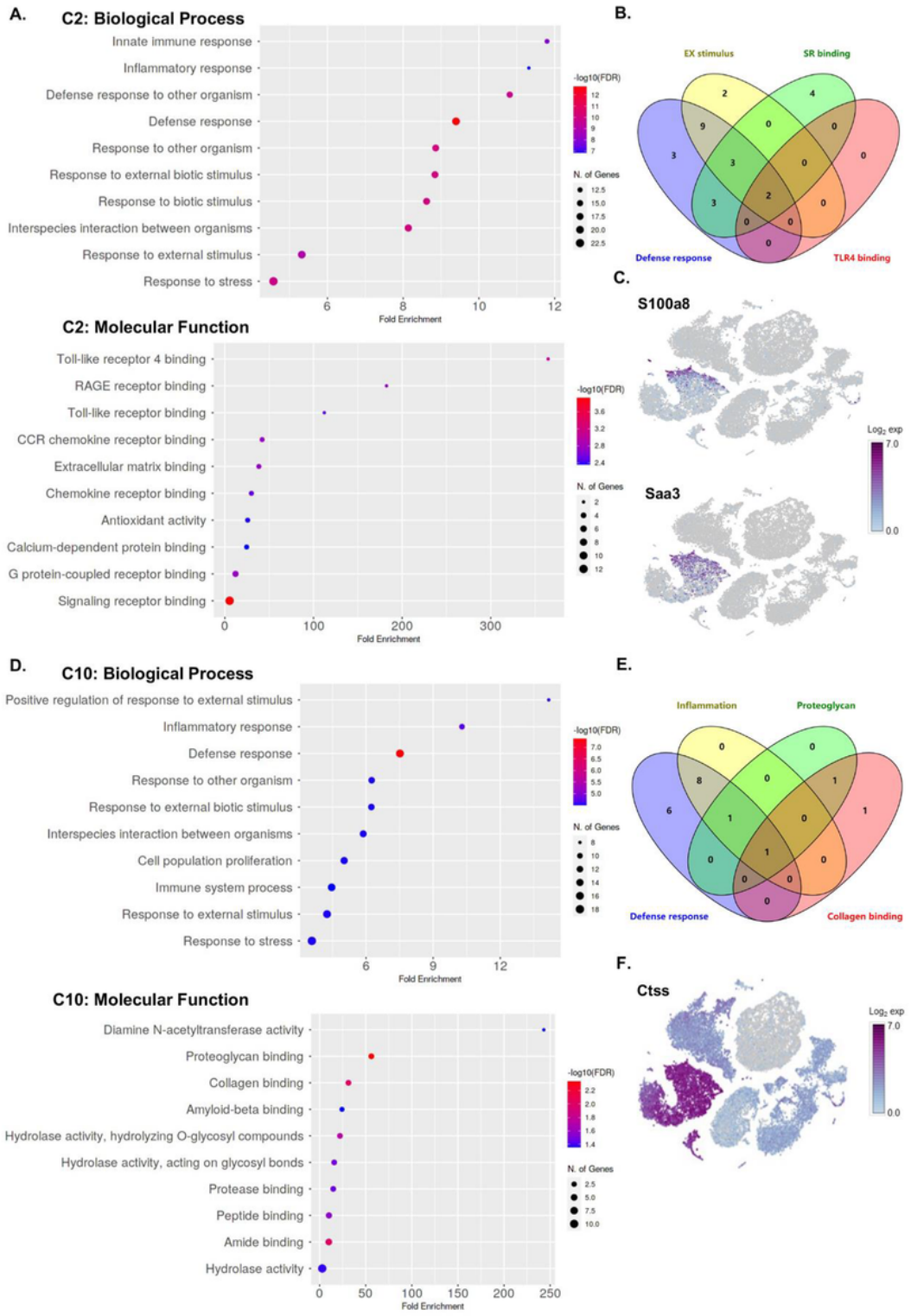

Figure 3

Gene functional analysis of cell cluster. (A) Biological process and molecular function analysis for cluster 2. (B)Combined analyze the genes in the above significant enrichment pathways to obtain two representative genes S100a8 and Saa3.EX stimulus, response to external stimulus; SR bingding, signaling receptor bingding.(C) Molecular distribution of S100a8 and Saa3. (D) Biological process and molecular function analysis Functional enrichment analysis for group cluster 10. (E) Combined analyze

the genes in the above significant enrichment pathways to obtain a representative genes CTSS. (F) Molecular distribution of CTSS.

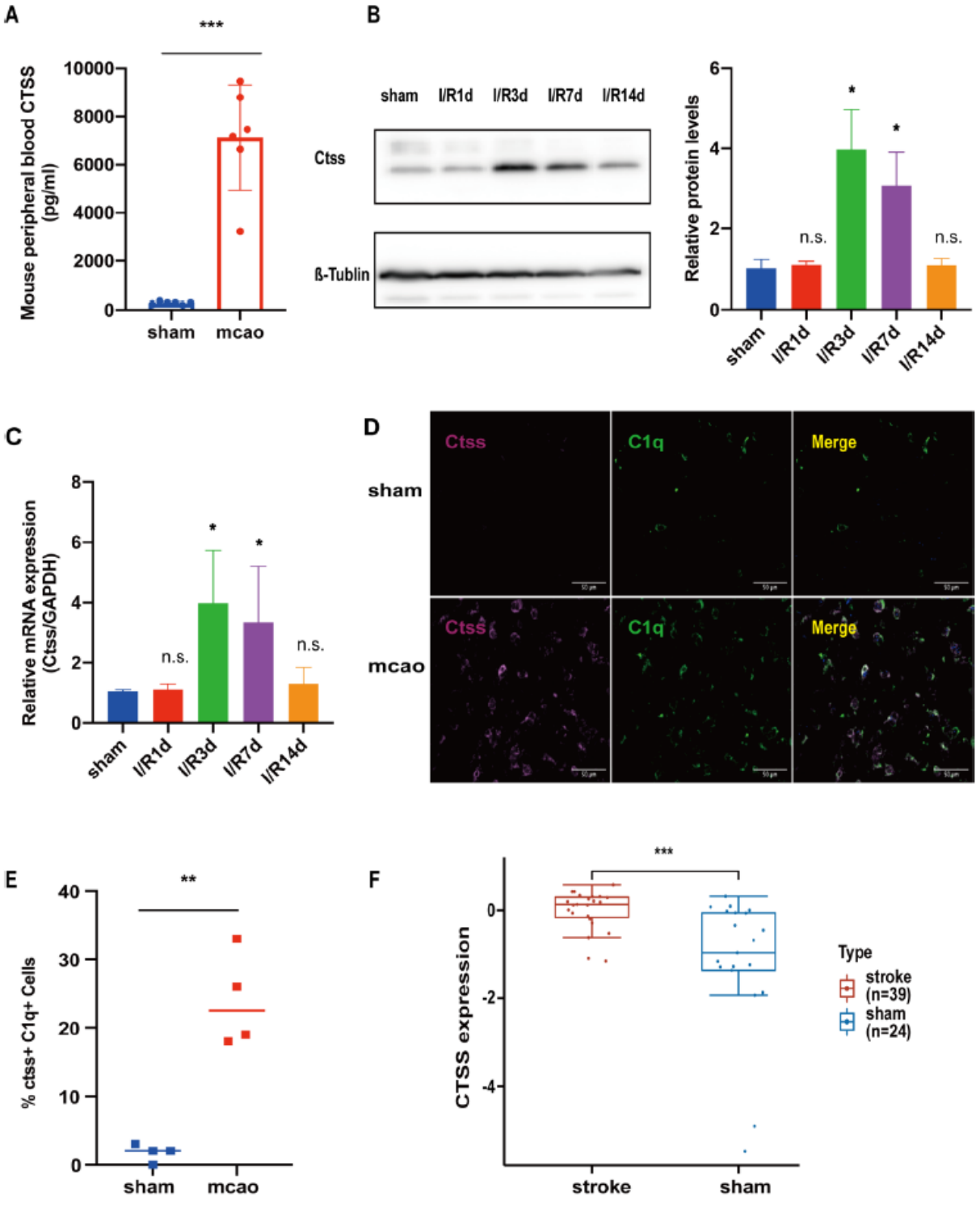

Figure 4

Circulating and cerebral CTSS are increased in mice after MCAO. C57BL/6N mice were subjected to sham operation or MCAO for 90 minutes followed by 1, 3, 7, and 14 days of reperfusion. (A) Serum CTSS levels

by ELISA after MCAO in mice (n = 6). (B) Representative immunoblots and quantification of CTSS (relative to GAPDH) in the ischemic ipsilateral brain at various time points after MCAO (n = 4). (C) The mRNA abundance of CTSS in the ischemic ipsilateral brain normalized to that of the GAPDH gene (n =5). (C and E) Representative images and quantitation of in situ hybridization results for CTSS and C1q in the sham group or 3 days after MCAO. (F) Serum CTSS levels after stroke in humans from GEO analysis database. All data represented as Mean ± SEM; *P < 0.05; **P < 0.01; ***P < 0.001; n.s. not significant.

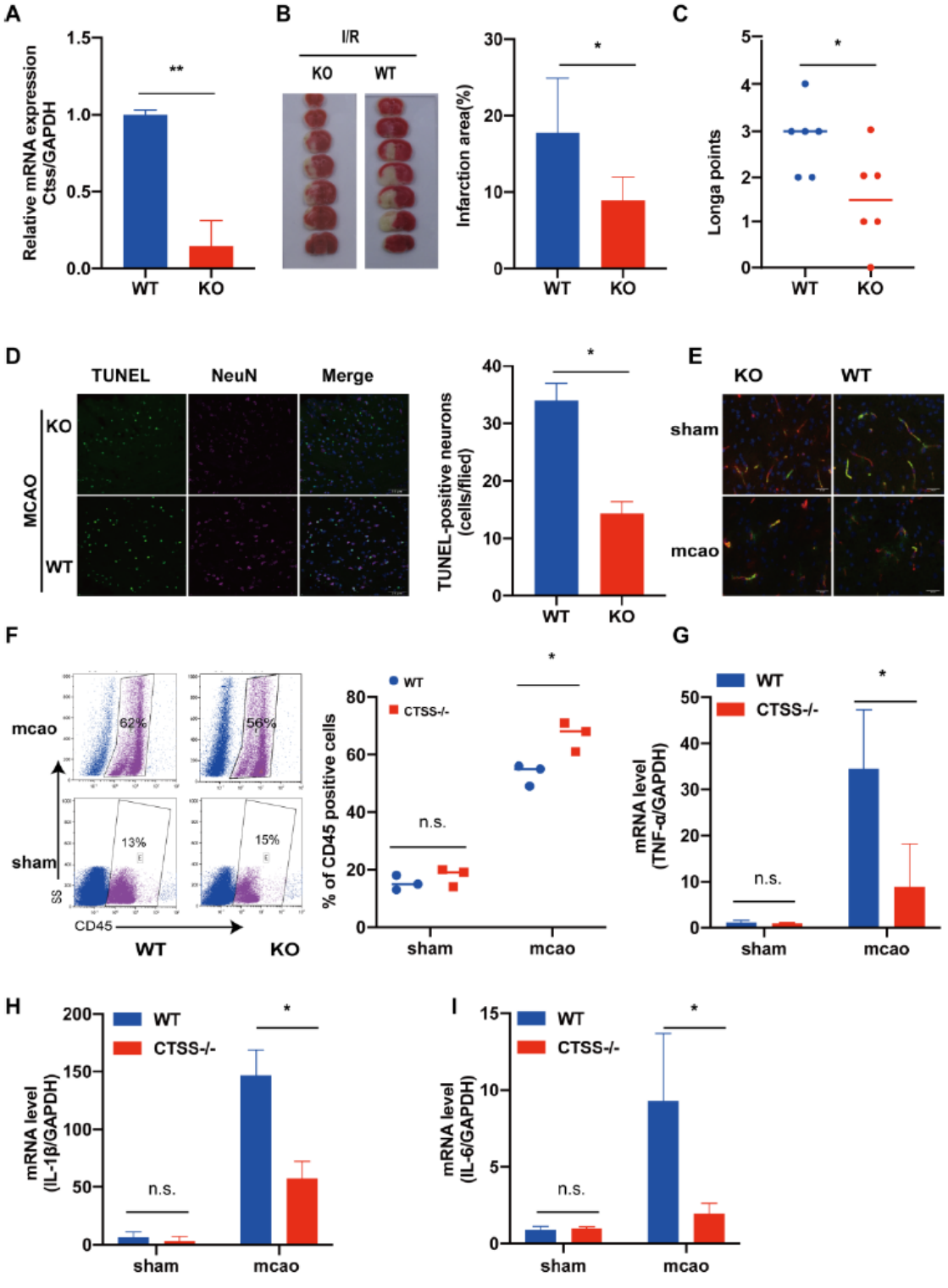

Figure 5

CTSS KO protects mice from cerebral ischemia injury. CTSS KO and WT mice (8 weeks old) were subjected to sham or MCAO for 90 minutes, followed by reperfusion for 3 days. (A) CTSS knockout efficiency by qRT-PCR. (B) Representative photographs of coronal brain sections of CTSS KO and WT mice stained with TTC after MCAO and the relative infarct volume (n = 5). (C) Neurological scores of CTSS KO and WT mice 3 days after MCAO. (D) Representative confocal images of TUNEL staining with the neuronal marker Neu-N in the ischemic brain in mice 3 days after MCAO and the quantification of TUNEL-positive neurons (n=3). (E) Representative confocal images of vascular permeability of WT and CTSS KO mice (green: thiocarbamoyl dextrans; red: CD31). (F) The number of total infiltrating $CD45^{hi}$ leukocytes in the brain according to flow cytometry (n=3). (G-I) Representative quantification of IL-1β, IL-6, TNF-α (relative to GAPDH) by qRT-PCR after MCAO(n=4). All data represented as Mean ± SEM; *P < 0.05; **P < 0.01; n.s. not significant.

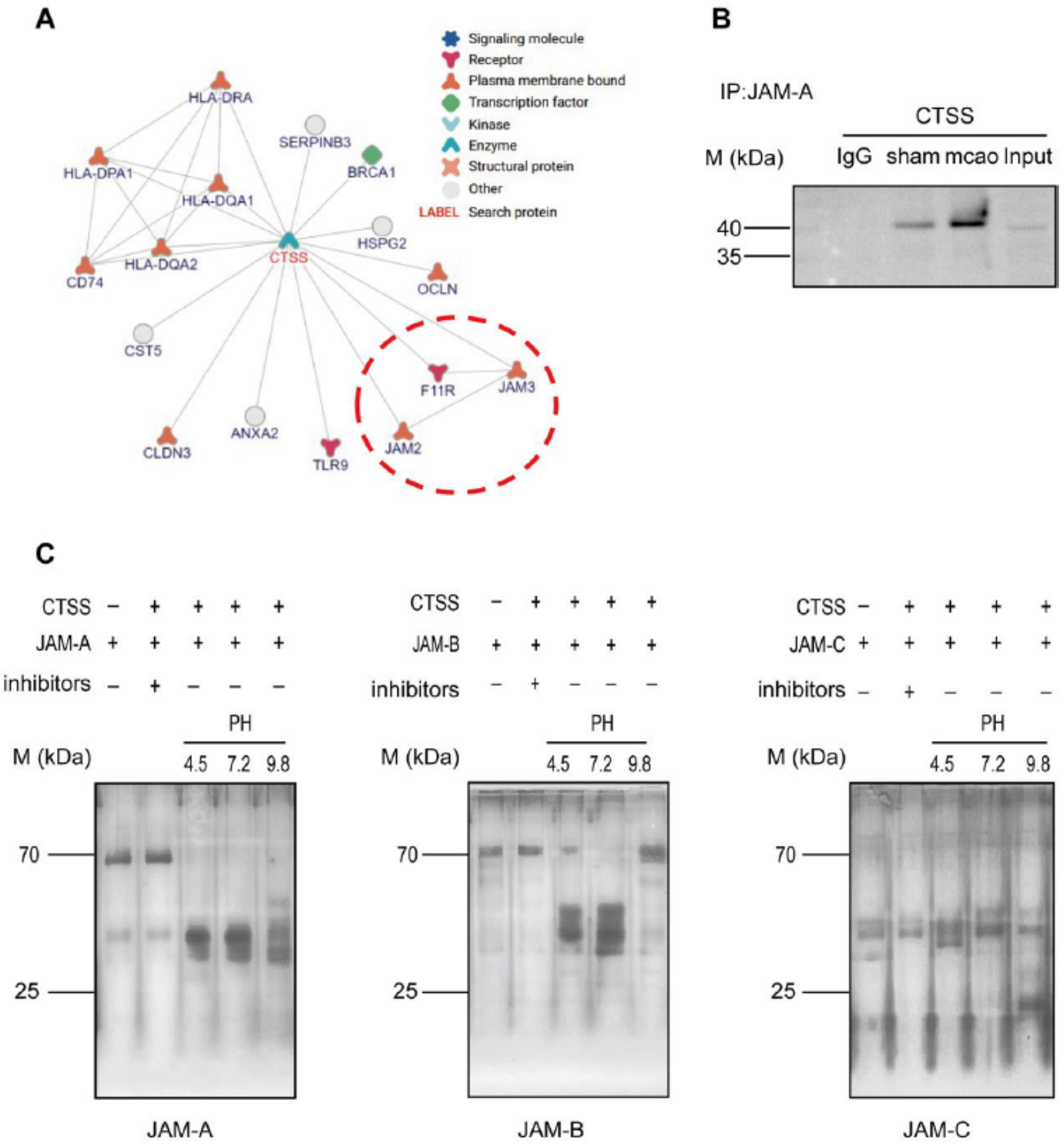

Figure 6

CTSS promotes the cleavage of vascular tight junction proteins in vitro. (A) Interaction prediction between JAM and CTSS. (B)Verification of the interaction between JAM-A and CTSS by CO-IP experiment. (C) Silver staining analysis of CTSS-mediated cleavage of recombinant tight junction proteins (JAM-A, JAM-B and JAM-C) at pH 4.8, pH 7.0 and pH 9.8 in the presence or absence of CTSS inhibitors.

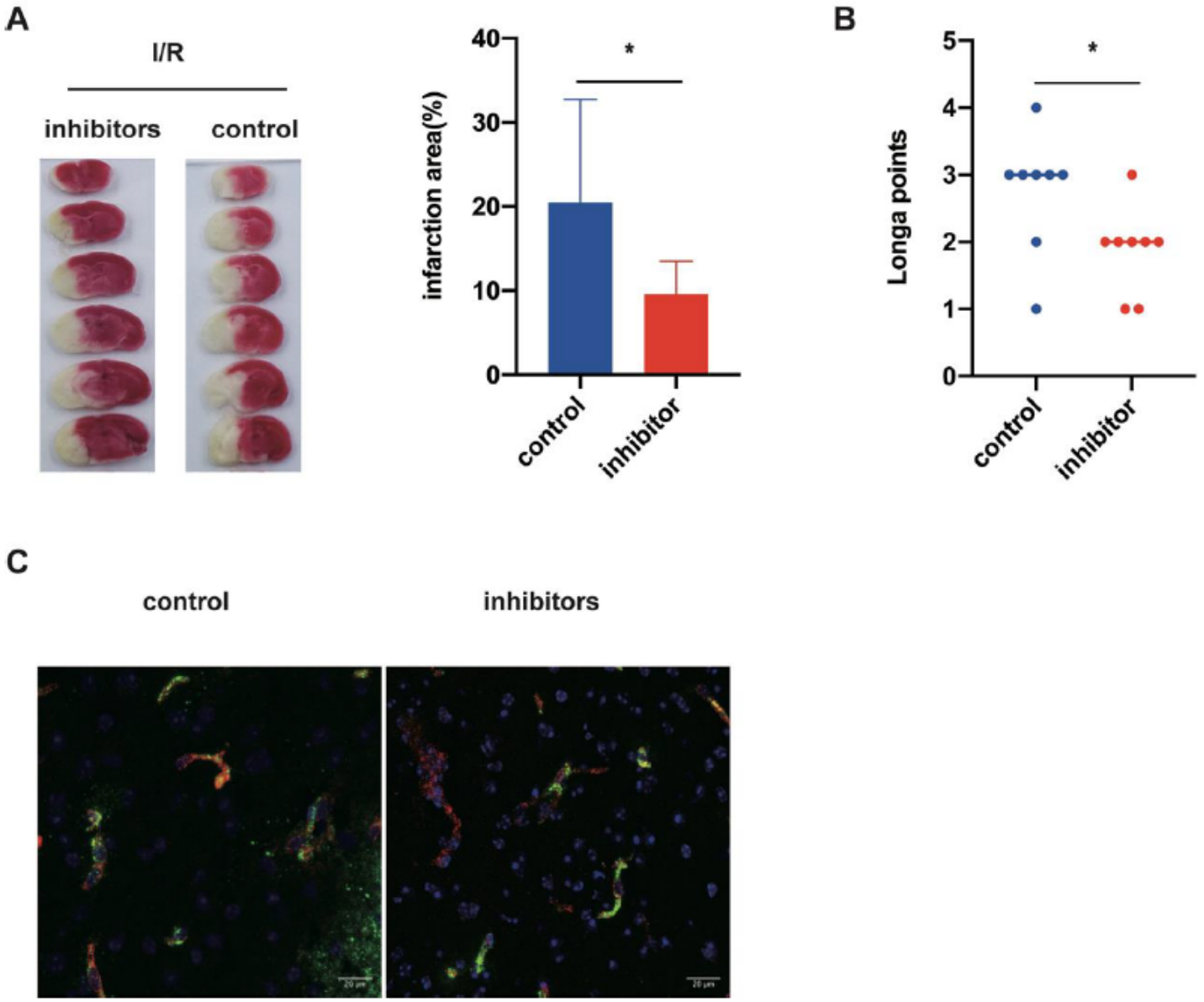

Figure 7

CTSS inhibitors protect mice from cerebral ischemia injury. (A) Representative photographs of coronal brain sections of mice stained with TTC after MCAO in inhibitors and control mice and the relative infarct volume (n = 8). (B) Neurological scores of inhibitor-treated and control mice 3 days after MCAO. (C) Representative confocal images of the vascular permeability of inhibitor-treated and control mice. All data represented as Mean ± SEM; *P < 0.05; **P < 0.01; ***P < 0.001; n.s. not significant.

Supplementary Files

This is a list of supplementary files associated with this preprint. Click to download.

- TableS1.xlsx

- TableS1.docx
- Additionalfilefigures.docx